Crystal structure of plant photosystem I

Adam Ben-Shem[1], Felix Frolow[2] & Nathan Nelson[1]

[1]*Department of Biochemistry and* [2]*Molecular Microbiology and Biotechnology, The George S. Wise Faculty of Life Sciences, Tel Aviv University, Tel Aviv 69978, Israel*

Oxygenic photosynthesis is the principal producer of both oxygen and organic matter on Earth. The conversion of sunlight into chemical energy is driven by two multisubunit membrane protein complexes named photosystem I and II. We determined the crystal structure of the complete photosystem I (PSI) from a higher plant (*Pisum sativum* var. *alaska*) to 4.4 Å resolution. Its intricate structure shows 12 core subunits, 4 different light-harvesting membrane proteins (LHCI) assembled in a half-moon shape on one side of the core, 45 transmembrane helices, 167 chlorophylls, 3 Fe–S clusters and 2 phylloquinones. About 20 chlorophylls are positioned in strategic locations in the cleft between LHCI and the core. This structure provides a framework for exploration not only of energy and electron transfer but also of the evolutionary forces that shaped the photosynthetic apparatus of terrestrial plants after the divergence of chloroplasts from marine cyanobacteria one billion years ago.

Oxygenic photosynthesis, the conversion of sunlight into chemical energy by plants, green algae and cyanobacteria, underpins the survival of virtually all higher life-forms. By producing oxygen and assimilating carbon dioxide into organic matter it determines to a large extent the composition of our atmosphere and provides essential food and fuel. This process is driven by PSI and PSII, two large multisubunit protein complexes that are embedded in the thylakoid membrane and act in series[1,2]. Photons absorbed by these complexes induce excitation of a special pair of chlorophylls initiating translocation of an electron across the membrane. This leads to the formation of an electrochemical potential, which powers ATP synthesis[3]. Water is the electron donor for this process and is oxidized to O_2 and four H^+ ions by PSII. The electrons extracted from water are shuttled through a quinone pool and the b_6f complex to plastocyanin, a small soluble copper protein[4]. Solar energy absorbed by PSI induces translocation of an electron from plastocyanin at the inner face of the membrane (lumen) to ferredoxin on the opposite side (stroma). The redox potential of ferredoxin is subsequently used in numerous regulatory cycles and reactions, including nitrate assimilation, fatty acid desaturation and NADPH production. In the dark, CO_2 reduction to carbohydrates is fuelled by ATP and NADPH chemical energy[5].

Plant PSI is composed of a reaction centre of up to 14 subunits and a membrane-associated antenna complex (LHCI) that captures light and guides its energy to the reaction centre[1]. On the whole, plant PSI binds approximately 200 pigments. Despite its complexity, PSI is highly efficient and almost every photon absorbed results in excitation of the special chlorophyll pair P_{700}[6]. LHCI consists of four different membrane proteins (Lhca1–4) with varying stoichiometry depending on light intensity and other environmental factors[7]. As all LHCI proteins share high sequence homology and spectral properties, the need for four different genes is not obvious[8]. LHCI proteins are unique among the chlorophyll-*a*/*b* binding proteins in their red-shifted absorbance and in the formation of dimers[9].

The cyanobacterial PSI is smaller in size compared with plant PSI, having a reaction centre that resembles the one in plants but with no peripheral antenna. Its structure (from *Synechococcus elongatus*) was recently published, providing detailed insights into the molecular architecture of this complex[10]. The model contained 12 protein subunits and 127 cofactors (96 chlorophyll *a*, 22 carotenoids, 2 phylloquinones, 3 Fe_4–S_4 clusters and 4 lipids). We sought to understand the interactions within LHCI and between it and the reaction centre, and to reveal how adjustment to a terrestrial habitat shaped the plant complex after divergence from marine cyanobacteria. To this end, we determined the X-ray crystal structure of PSI from peas and describe here a model at 4.4 Å resolution.

Overall architecture

Plant PSI is monomeric both *in vitro* and *in vivo*[11,12]. A view from the stroma of the plant PSI Cα backbone (Fig. 1a) reveals that the reaction centre and LHCI form two distinct and loosely associated moieties, with a deep cleft between them. The four antenna proteins assemble into two dimers, arranged in a series, creating a half-moon-shaped belt that docks to the reaction centre's subunit F side. We assigned (see Supplementary Information) these two dimers to Lhca1–Lhca4 and Lhca2–Lhca3 (Fig. 1a) according to published biochemical and mutagenic studies[13–17]. The LHCI belt, with its associated chlorophylls, is the most prominent addition to the PSI structure made by plants (and green algae). It contributes a mass of 150 kDa out of approximately 525 kDa. The plant reaction centre moiety retains the location and orientation of the electron transfer components and all cyanobacterial transmembrane helices, except those of subunits X and M (not present in plants). In addition to these retained features, four reaction centre proteins are present exclusively in plants and green algae (subunits G, H, N, O; see refs 12, 18). Two of these, namely G (PsaG) and H (PsaH), both membrane proteins of 10 kDa, are revealed in our model (Fig. 1a, b). A single transmembrane helix adjacent to PsaL was assigned to PsaH in agreement with cross-linking data[13]. This transmembrane segment is followed by a 20-Å-long helix lying parallel to the membrane, coordinating one chlorophyll molecule (Fig. 2a). The position and shape of PsaH conforms well to its proposed role as a docking site for LHCII[19]. On the opposite side of the reaction centre PsaG, with its two tilting transmembrane helices, contributes most of the contact surface area for association with LHCI (Fig. 2a).

On the luminal side, the most noticeable distinction between plant and cyanobacterial reaction centres is the helix–loop–helix motif contributed by the longer amino-terminal domain of plant PsaF (Fig. 1b). This domain enables the more efficient plastocyanin binding in plants and, as a result, two orders of magnitude faster electron transfer from this copper protein to P_{700}[20].

Conservation of chlorophyll positions in the PSI core

Recent phylogenetic studies and whole-genome analyses depict an evolutionary model in which oxygen-evolving cyanobacteria originated after the divergence of Bacteria from Archaea, becoming prevalent around 2.5 billion years ago, and coinciding with the earliest rise in oxygen levels on Earth[21,22]. Since chloroplasts diverged from their cyanobacterial ancestors, at least 1 billion years ago, they have undergone a separate evolution. It is therefore remarkable that in the structure of the plant PSI reaction centre, we find that the positions of virtually all of the cyanobacterial chlorophylls are almost precisely preserved (Fig. 2b). During 1 billion years of evolutionary processes an enormous number of random

mutations took place, yet both cyanobacteria and higher plants maintained the same chlorophyll arrangement. Out of the 96 chlorophyll molecules reported in the model of the cyanobacterial PSI reaction centre only three are missing in the plant PSI reaction centre: two bound to PsaM and PsaX, and one bound to PsaJ. From the remaining 93 chlorophylls, 92 are identified at the same position in the plant reaction centre, including 15 chlorophylls with their Mg^{2+} coordinated by water (Fig. 2a, b and ref. 10). It is noteworthy that among the more peripheral chlorophylls of the reaction centre, which probably do not transfer energy directly to P_{700}, we find only one that is not conserved in the plant complex (*J*3) and only one other where a significant positional modification occurs (*B*33). A few other minor alterations, mainly in chromophore orientation, are also observed. Thus, adaptation of the reaction centre to the utilization of energy from the LHCI antenna only required the addition of ten chlorophyll molecules at the three 'contact regions', as discussed below (Fig. 2c).

Formation of the LHCI belt and its binding to the core

What are the interactions giving rise to the formation of the two

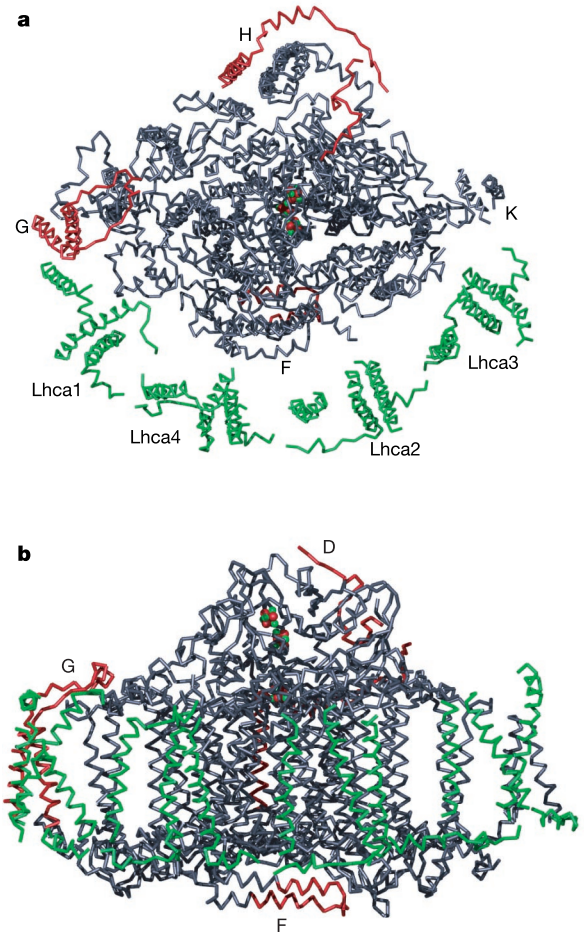

Figure 1 The structural model of plant PSI at 4.4 Å represented as Cα backbone. The four light-harvesting proteins are in green (Lhca1–4). Novel structural elements within the reaction centre (core) that are not present in the cyanobacterial counterpart are coloured red; conserved features of the reaction centre are in grey. The three Fe_4–S_4 clusters are depicted as red (Fe) and green (S) balls. **a**, View from the stromal side of the thylakoid membrane. Subunits F, G, H and K of the reaction centre are indicated. The assignment of the four different Lhca proteins is shown. **b**, A view from the LHCI side. Subunits F, G and D are indicated. The helix–loop–helix N-terminal domain of subunit F and the N terminus of subunit D unique to plant photosystem I are coloured red.

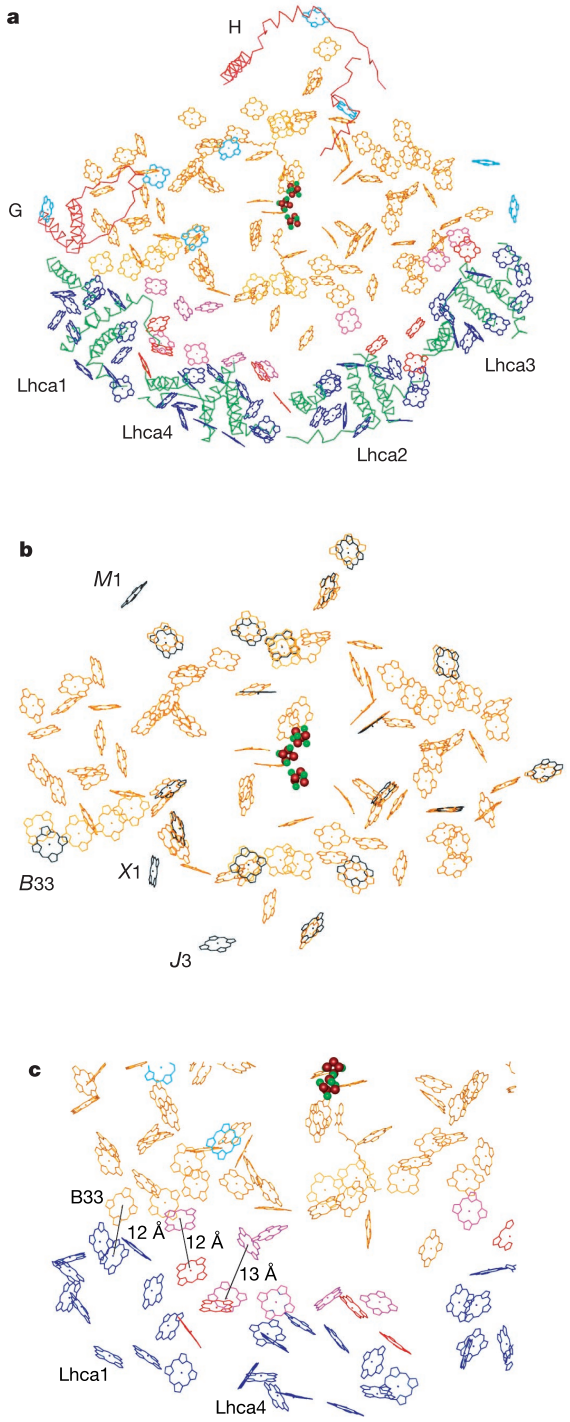

Figure 2 The arrangement of 167 chlorophyll molecules of plant PSI as seen from the stromal side. Yellow, plant reaction centre chlorophylls that are present in cyanobacteria; cyan, reaction centre chlorophylls unique for plants; blue, chlorophylls bound to the Lhca monomers; red, LHCI linker chlorophylls (see text); magenta, chlorophylls positioned in the cleft between LHCI and the reaction centre (designated as gap chlorophylls in the text). **a**, Chlorophyll arrangement including Cα backbone of subunits that are exclusive to eukaryotic PSI. **b**, Conservation of cyanobacterial reaction centre chlorophylls in plant. The cyanobacterial chlorophylls that are missing or that have changed their position or orientation in plant reaction centre are in black. **c**, The contact region between the LHCI belt and the reaction centre in the vicinity of subunit G and Lhca1. Shortest Mg^{2+}–Mg^{2+} distances between LHCI belt and core chlorophylls are indicated.

LHCI dimers? We find that helix D at the luminal carboxy-terminal domain of Lhca1 protrudes out of the main body of this protein and binds to both helix C and the luminal loop, connecting helices C and B, of Lhca4 (Fig. 3a). A similar, but apparently weaker, binding mode appears between Lhca2 and Lhca3, and also between the two dimers. The mode of binding depicted in Fig. 3a underlines the importance of the C-terminal domain of Lhca1 for dimer formation[16], and suggests a similar role for the N terminus. Hence, the LHCI proteins are arranged in a series where helix D of one monomer is pointing towards helix C of the next. This maximizes the number of LHCI chlorophylls facing the core. It is noteworthy that the loops connecting the transmembrane helices are the least conserved between LHCI and trimer-forming LHCII[23,24]. In spite of this dimerization mode, which does not involve interactions between transmembrane helices, the interpigment distances between the nearest chlorophylls of neighbouring monomers are still very short. This is due to the 'linker' chlorophylls, located between the monomers, which may have an important role in energy migration along the LHCI belt (Figs 2a and 3a). The possible physical interaction with chlorophylls at the interfaces between LHCI monomers suggests that the linker chlorophylls could also be important for dimer formation.

As expected from the amino acid sequences, the helix structure of LHCI (Fig. 4a–d) and LHCII[23] is quite similar. All four LHCI monomers share the LHCII general fold; that is, two long, tilted, intertwined transmembrane helices (A and B), a shorter one roughly perpendicular to the membrane (C), and a 10–12-amino-acid-long hydrophilic helix parallel to the luminal membrane (D). In terms of absorption characteristics, the main distinction between LHCI and LHCII is the longer wavelength absorption spectrum. This difference is mainly attributable to tighter interactions between pigments in LHCI; however, protein–pigment interactions may also contribute[25]. The structure reveals that although the positions, number of chlorophylls and Mg^{2+}–Mg^{2+} distances in LHCI monomers are similar to those in LHCII, there are a few marked alterations particularly in chromophore orientations (Fig. 4c, d). Most noticeable are the sharp differences in the tilting of chlorophylls *b*5 (or *a*5), *a*7 and *a*3 (see ref. 23 for nomenclature), as well as the modified location of chlorophyll *b*2, which in LHCI is positioned closer and parallel to a linker chlorophyll located between two monomers. All these chlorophylls face either the core or the neighbouring monomer. The most prominent distinction in chlorophyll arrangement between LHCI and LHCII is not to be found in the isolated monomers (Fig. 4b, d). Within each dimer, two linker chlorophylls are bound at the interface between the neighbouring monomers and one chlorophyll is located between the two dimers. In addition, another linker chlorophyll, which appears in all four LHCI proteins, is positioned close to chlorophyll *a*4 and faces the reaction centre.

Binding of LHCI to the reaction centre is asymmetric; that is, much stronger on the G-pole than on the K-pole of the core (Fig. 1a). Lhca1 is strongly attached to the core through the helix bundle formed between its transmembrane helix C and the two tilted helices of PsaG, and owing to the close interaction of its stromal loop with the novel loop 1 of PsaB (Fig. 3b). The other LHCI proteins interact with the core mainly through small binding surfaces at their stromal-exposed regions (Fig. 1a). Lhca4 binds to PsaF, Lhca2 associates weakly with PsaJ, and Lhca3 interacts with an unassigned electron density that is probably attributable to the stromal loop of PsaK (on the luminal side Lhca3 binds weakly to PsaA). This observation fits in with recent work concerning alterations of LHCI composition with changing environmental conditions[7,26]. We suggest that Lhca1, and to some extent the Lhca1–Lhca4 dimer, act as an anchor point for facilitating the binding of other LHCI monomers and dimers (and their isoforms) at varying

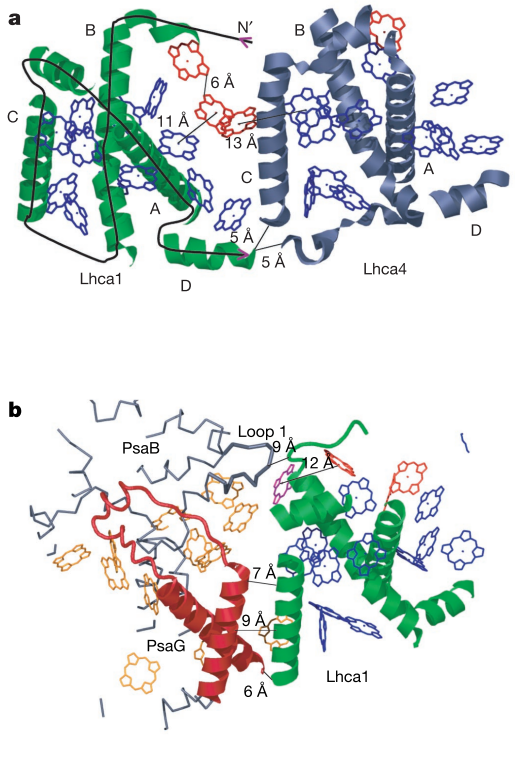

Figure 3 Dimer formation between Lhca1 and Lhca4 and tight binding of Lhca1 to the reaction centre. **a**, The close contact between helix D of Lhca1 (green) and both the luminal region of helix C and the luminal loop connecting helices B and C of Lhca4 (grey) is shown. The magenta solid line follows schematically the Lhca1 backbone from the putative N terminus (N′) to the C terminus. Chlorophyll colour code is as in Fig. 2. The nomenclature for the four helices (A, B, C and D) is adopted from LHCII[23]. **b**, Tight binding of Lhca1 to subunits B and G of the reaction centre.

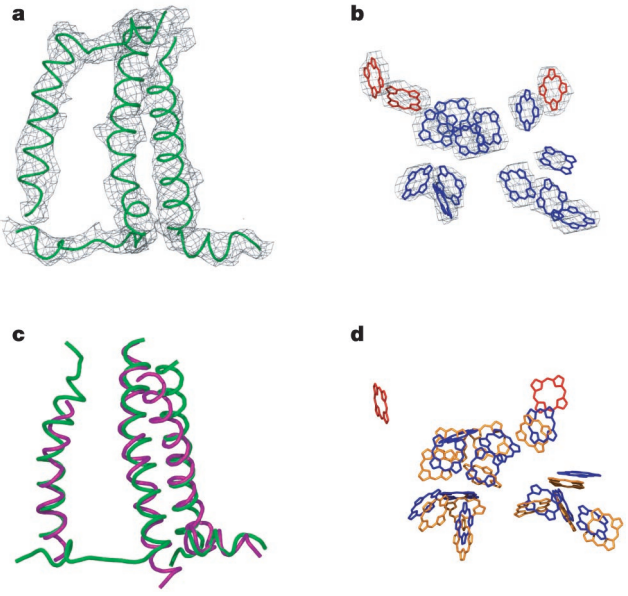

Figure 4 The structural model of Lhca monomers compared to LHCII. **a**, The experimental electron density map covering the Cα backbone of Lhca4. **b**, Experimental electron density map covering the chlorophylls of Lhca4. Chlorophylls in blue have parallels in LHCII whereas the additional linker chlorophylls (see text) are in red. **c**, Superposition of Lhca2 (green) and LHCII (magenta) backbones. **d**, Superposition of the chlorophylls of Lhca2 (blue and red) and LHCII (yellow). Note that this Lhca contains only two linker chlorophylls.

stoichiometries, depending on environmental conditions. Our structure therefore suggests that an important function unique to each Lhca protein is the fine-tuned and tailor-made interactions that it has with the core and other Lhca monomers.

Chlorophyll arrangement and excitonic energy transfer

The four LHCI proteins are evenly spaced along the antenna belt, with virtually identical distances between dimers and dimer subunits (Fig. 1a). The belt is densely populated with chlorophylls. Within the membrane, the Cα backbone of LHCI maintains a distance of more than 20 Å from most parts of the reaction centre. Owing to this gap, most LHCI chlorophylls are separated by more than 18 Å from the nearest reaction centre chlorophyll (Mg^{2+}–Mg^{2+} distances). However, there are three contact regions where much shorter interpigment distances (10–15 Å) are observed, and these are proposed to play an important role in energy migration. These denser contact regions are located at the two poles of the LHCI belt near PsaK and PsaG (Fig. 2a, c), with an additional minor region located at the centre of the LHCI belt in the vicinity of PsaF. Core chlorophylls that are not present in cyanobacteria, or antenna chlorophylls that have no counterparts in LHCII, are involved in most of the chlorophyll pairs forming the closer interactions. Apparently, optimization of energy transfer between LHCI and the core arose through the evolution of a small number of strategically positioned chlorophyll-binding sites that we designate as 'gap' chlorophylls. Except for the described linker chlorophylls, which are intimately associated with LHCI, ten additional gap chlorophylls are not an intrinsic part of the LHCI belt or the reaction centre. They are bound to the periphery of either one or both of these moieties and are positioned within the cleft between them. The non-uniform distribution of close LHCI–core contacts among the three contact regions suggests the existence of distinct energy migration routes from the antenna to the core of PSI.

The chlorophyll arrangement described here, where most antenna chlorophylls are located 20–32 Å from core chlorophylls (Mg^{2+}–Mg^{2+} distance) except at the contact regions, resembles the architecture of chlorophyll distribution in the reaction centre. There, the innermost chlorophylls are all distanced 20–30 Å from the electron transfer chain, except for two linker chlorophylls that are positioned at greater proximity to it. This arrangement maximizes the number of chlorophylls that can deliver energy directly to the electron transfer chain.

Here we show that the LHCI belt is much more densely populated than previously estimated[27]. With its 56 chlorophylls (not including gap chlorophylls), the ratio of chlorophyll/protein exceeds even that of the reaction centre or LHCII. Such a high pigment density, yielding a more intricate set of close pigment–pigment interactions (Fig. 2a), may be responsible for LHCI's unique spectral characteristics. LHCI harbours most of the red-shifted chlorophylls of plant PSI[28]. These are of considerable importance for light harvesting in dense vegetation systems, where ambient light is enriched in wavelengths above 690 nm (ref. 29). Energy from these chlorophylls migrates to neighbouring bulk chlorophylls through a slow, thermally activated transfer that reduces the rate of energy migration from the antenna to the core[30]. The enhanced pigment–pigment

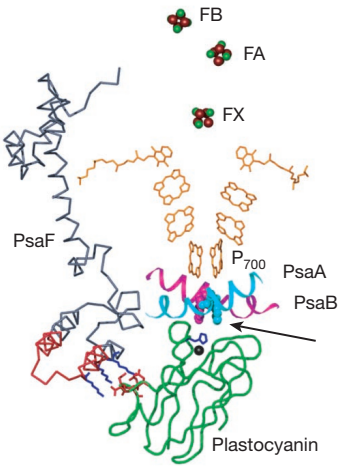

Figure 5 Electron transfer chain and plastocyanin binding. Residues 18–47 of plant PsaF, which include the 18 residues exclusive to eukaryotes and that form a helix–loop–helix domain, are coloured red. A cluster of four negatively charged residues (red) on the surface of plastocyanin (green) interacts with three lysines (blue) from the N terminus of PsaF, two of which are from the extra 18 residues. The two tryptophan residues (indicated by an arrow) crucial for the electron transfer from the reduced copper to the oxidized P_{700}, and that contribute to the hydrophobic interaction with plastocyanin, are shown as spherical atoms (cyan and magenta). The histidine residue that coordinates the copper atom in plastocyanin is in blue.

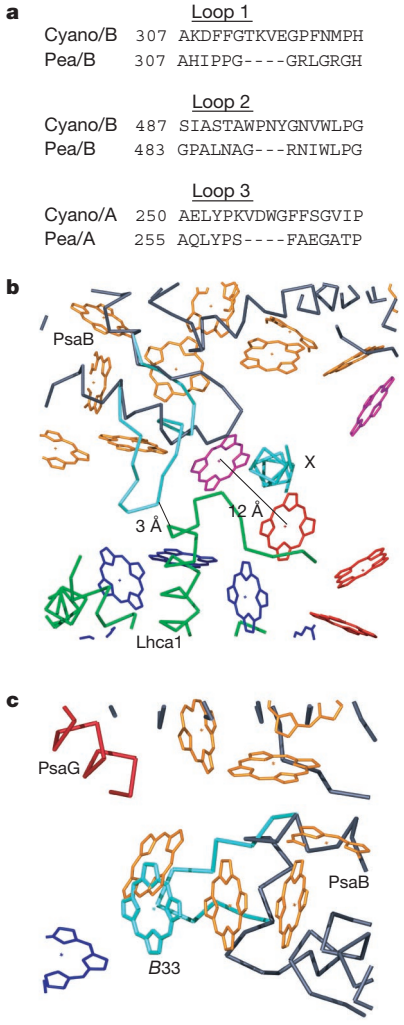

Figure 6 Loops altered during the evolution of plant PsaA and PsaB. The cyanobacterial domains modified or eliminated in plants are in cyan; plant Cα backbone is in grey; and the colour code of the various plant chlorophylls is as in Fig. 2. **a**, Amino acid sequence alignment of the regions that accommodate the three altered loops. **b**, Loop 1. This stromal loop was altered and subunit X was eliminated in the plant reaction centre. The altered loop coordinates a gap chlorophyll positioned close to Lhca1 chlorophyll (distance indicated). **c**, Loop 2. Modification of loop 2 results in a large change in the position of chlorophyll *B*33 that in *S. elongatus* (cyan) forms part of a trimer of parallel chlorophylls that was proposed to absorb light at longer wavelengths.

interaction in LHCI may decrease the time required for the slow 'uphill' push from low-energy chlorophylls by providing many possible acceptors in their vicinity.

Plastocyanin binding and electron transfer

Plastocyanin is the only electron donor of plant PSI, and PsaF is known to provide part of the plastocyanin-binding site[20,31]. Figure 5 depicts a model of plastocyanin- and plant PSI-binding, based on our model of PSI and the available structure of plastocyanin (Protein Data Bank code 1ag6)[32]. In this model, plastocyanin's positioning in the putative binding site was guided by hydrophobic interactions between a region of plastocyanin, proximal to the copper ion, with the luminal loops containing Trp 625 in PsaB and Trp 658 in PsaA (Fig. 5 and ref. 33). Superfluous degrees of freedom have been resolved by bringing into contact a cluster of negatively charged conserved residues (Asp 42, Glu 43, Asp 44 Glu 45) of plastocyanin with the positively charged N-terminal domain of PsaF, which contains a few lysine residues that are not present in cyanobacteria[20,34]. This arrangement brings the copper atom in plastocyanin to coincide with the pseudo two-fold axis of symmetry of the electron transfer path from the special chlorophyll pair (P_{700}) to the Fe_4–S_4 cluster Fx.

Electron transfer from plastocyanin to PSI is two orders of magnitude faster in plants compared with cyanobacteria[20]. This is probably due to more efficient plastocyanin binding in plants, mediated by the extra 18 amino acid residues in the N terminus of plant PsaF (Fig. 1b). This extra N-terminal domain forms an amphipathic helix–loop–helix motif on the luminal side of the thylakoid membrane (Fig. 5). Sequence alignment and the good match between our electron density map and the cyanobacterial model outside this region allowed us to place the known sequence of the extra 18 residues within this luminal helix–loop–helix. One of these helices contains two lysine residues—Lys 30 and to a greater extent Lys 23—that are responsible for the much stronger electrostatic interaction between plastocyanin and PSI[35].

Evolutionary forces shaping plant PSI

Sequence alignment of the core main subunits A and B between plants and *S. elongatus* revealed only three sites where amino acids were lost in plants (Fig. 6a). They all form parts of solvent-exposed loops denoted loop 1, loop 2 and loop 3. As depicted in Fig. 6b, closer association of Lhca1 with the core probably arose through modification of the protruding cyanobacterial loop 1 and elimination of PsaX. The resulting smaller loop binds Lhca1 and coordinates a gap chlorophyll that might have a role in energy migration from this antenna protein to the core. Similarly, modification in the protruding cyanobacterial loop 3 enabled closer association of Lhca3 with the core (not shown). Alteration of loop 2 (Fig. 6c) results in a substantial change in the position of chlorophyll *B*33 that, together with *B*31 and *B*32, forms in *S. elongatus* a strongly coupled trimer to which absorption at the end of its range in the red-light wavelength is attributed[10]. This modification is therefore probably manifested in the different absorption spectra of the plant reaction centre. This is the only instance where the position of cyanobacterial chlorophyll changed significantly in the plant core: note that it takes place at one of the contact regions.

Whereas plant PSI is purified as a monomer its cyanobacterial counterpart assembles *in vivo* into trimers[1]. By superimposing three plant PSI monomers on top of the cyanobacterial trimer we are able to conclude unequivocally that plant PSI cannot form similar trimers because its PsaH, not present in cyanobacteria, completely hinders the formation of contacts among the monomers. As PsaH probably forms part of the docking site for LHCII it implies that trimerization was lost in plants to facilitate re-allocation of phosphorylated LHCII to PSI under light conditions favouring PSII excitation. Furthermore, we find that the C terminus of PsaL, which protrudes in the cyanobacterial reaction centre and facilitates trimer formation, is lost in plants. Again, as in loop 1 and loop 3, we suggest that association with a membrane antenna protein, in this case LHCII, forced the elimination of a protruding domain.

Recently it was discovered that under certain stress conditions, not uncommon to a marine habitat, the cyanobacterial PSI is also augmented by a membrane antenna protein called CP43′ (unrelated to LHCI monomers but related to CP43 from PSII). Eighteen identical copies of CP43′ form a circle around the periphery of the PSI trimer, which keeps an almost constant distance from the core (on its F/J side) except for three closer interaction regions per monomer[36–38]. As this circle is energetically efficiently coupled to the reaction centre[39], we hypothesize that the cyanobacterial reaction centre is optimized not only for a 'stand alone' set up but also for trapping energy delivered from a peripheral membrane antenna. This might explain the paucity of alterations that plant reaction centre chlorophylls had to undergo.

The major differences in the overall architecture of the LHCI and CP43′ belts may reflect the need of plants to adjust to an environment with a different light regime and where light intensity and quality are subject to much greater dynamic variations[7,29]. In the LHCI belt, chlorophyll density is almost double that of the CP43′ belt. This higher density gave rise to the red-shifted chlorophylls that broadened the plant PSI absorption spectra. It also enabled placing the belt of chlorophylls much closer to the core (interpigment distances between core and belt in the three contact regions are 20–25 Å in PSI–CP43′ compared with 10–15 Å in LHCI–PSI). This proximity, made possible by eliminating some cyanobacterial protruding loops, might be essential in compensating for the red chlorophylls that significantly reduce the rate of energy migration to the core. LHCI is composed of four different building blocks that change their composition in response to varying environmental conditions. This flexibility in LHCI stoichiometry is facilitated by the strong binding of Lhca1 to PsaG, the looser association of the other Lhca monomers to the core, and the relatively weak interaction between the Lhca proteins.

The structure of plant PSI presented here reveals the spatial distribution of all of its transmembrane helices and the vast majority of the cofactors involved in energy and electron transfer. It provides a framework for further investigation of the mechanisms regulating the composition and activity of PSI's numerous subunits under changing environmental conditions. □

Methods

PSI was isolated as a monomer from fresh pea (*Pisum sativum* var. *alaska*) leaves and crystallized as described elsewhere[11,40] in space group $P2_1$, with unit-cell parameters $a = 181.90$ Å, $b = 190.24$ Å, $c = 219.66$ Å, $\beta = 90.48°$, exhibiting diffraction to 4 Å resolution at a synchrotron source. Phases were determined using several heavy-atom derivatives and the anomalous signal of the intrinsic Fe–S clusters. Figure of merit converged to 0.43 before and 0.71 after density modification. The asymmetric unit contains two PSI copies related by non-crystallographic symmetry that cannot occur *in vivo* within the membrane. The final electron density map allowed tracing of all transmembrane helices (modelled by polyalanine), and some additional structural elements, as well as determination of the position and tilting of the vast majority of chlorophylls (modelled by porphyrins). The final model was refined as a rigid body yielding $R = 0.41$ and $R_{free} = 0.42$. Supplementary Table 1 provides detailed information about the X-ray data collection and phasing. The conserved parts of plant and cyanobacterial reaction centres were handled as described in the Supplementary Methods.

Received 21 August; accepted 28 October 2003; doi:10.1038/nature02200.

1. Chitnis, P. R. Photosystem I: Function and physiology. *Annu. Rev. Plant Physiol. Plant. Mol. Biol.* **52,** 593–626 (2001).
2. Barber, J. Photosystem II: a multisubunit membrane protein that oxidises water. *Curr. Opin. Struct. Biol.* **12,** 523–530 (2002).
3. Junge, W. ATP synthase and other motor proteins. *Proc. Natl Acad. Sci. USA* **96,** 4735–4737 (1999).
4. Cramer, W. A. *et al.* Some new structural aspects and old controversies concerning the cytochrome b(6)f complex of oxygenic photosynthesis. *Annu. Rev. Plant Physiol. Plant Mol. Biol.* **47,** 477–508 (1996).
5. Herrmann, R. G. Biogenesis and evolution of photosynthetic (thylakoid) membranes. *Biosci. Rep.* **19,** 355–365 (1999).
6. Trissl, H.-W. & Wilhelm, C. Why do thylakoid membranes from higher plants form grana stacks? *Trends Biochem. Sci.* **18,** 415–419 (1993).
7. Bailey, S., Walters, R. G., Jansson, S. & Horton, P. Acclimation of *Arabidopsis thaliana* to the light environment: the existence of separate low light and high light responses. *Planta* **213,** 794–801 (2001).

8. Durnford, D. G. *et al.* A phylogenetic assessment of the eukaryotic light-harvesting antenna proteins, with implications for plastid evolution. *J. Mol. Evol.* **48,** 59–68 (1999).
9. Croce, R., Morosinotto, T., Castelletti, S., Breton, J. & Bassi, R. The Lhca antenna complexes of higher plants photosystem I. *Biochim. Biophys. Acta* **1556,** 29–40 (2002).
10. Jordan, P. *et al.* Three-dimensional structure of cyanobacterial photosystem I at 2.5 Å resolution. *Nature* **411,** 909–917 (2001).
11. Ben-Shem, A., Nelson, N. & Frolow, F. Crystallization and initial X-ray diffraction studies of higher plant photosystem I. *Acta Crystallogr. D* **59,** 1824–1827 (2003).
12. Scheller, H. V., Jensen, P. E., Haldrup, A., Lunde, C. & Knoetzel, J. Role of subunits in eukaryotic Photosystem I. *Biochim. Biophys. Acta* **1507,** 41–60 (2001).
13. Jansson, S., Andersen, B. & Scheller, H. V. Nearest-neighbor analysis of higher-plant photosystem I holocomplex. *Plant Physiol.* **112,** 409–420 (1996).
14. Kargul, J., Nield, J. & Barber, J. Three-dimensional reconstruction of a light-harvesting complex I-photosystem I (LHCI-PSI) supercomplex from the green alga *Chlamydomonas reinhardtii*. Insights into light harvesting for PSI. *J. Biol. Chem.* **278,** 16135–16141 (2003).
15. Ihalainen, J. A. *et al.* Pigment organization and energy transfer dynamics in isolated photosystem I (PSI) complexes from *Arabidopsis thaliana* depleted of the PSI-G, PSI-K, PSI-L, or PSI-N subunit. *Biophys. J.* **83,** 2190–2201 (2002).
16. Schmid, V. H., Paulsen, H. & Rupprecht, J. Identification of N- and C-terminal amino acids of Lhca1 and Lhca4 required for formation of the heterodimeric peripheral photosystem I antenna LHCI-730. *Biochemistry* **41,** 9126–9131 (2002).
17. Ganeteg, U., Strand, A., Gustafsson, P. & Jansson, S. The properties of the chlorophyll a/b-binding proteins Lhca2 and Lhca3 studied *in vivo* using antisense inhibition. *Plant Physiol.* **127,** 150–158 (2001).
18. Knoetzel, J., Mant, A., Haldrup, A., Jensen, P. E. & Scheller, H. V. PSI-O, a new 10-kDa subunit of eukaryotic photosystem I. *FEBS Lett.* **510,** 145–148 (2002).
19. Lunde, C. P., Jensen, P. E., Haldrup, A., Knoetzel, J. & Scheller, H. V. The PSI-H subunit of photosystem I is essential for state transitions in plant photosynthesis. *Nature* **408,** 613–615 (2000).
20. Hippler, M. *et al.* The plastocyanin binding domain of photosystem I. *EMBO J.* **15,** 6374–6384 (1996).
21. Raymond, J., Zhaxybayeva, O., Gogarten, J. P., Gerdes, S. Y. & Blankenship, R. E. Whole-genome analysis of photosynthetic prokaryotes. *Science* **298,** 1616–1620 (2002).
22. Xiong, J. & Bauer, C. E. Complex evolution of photosynthesis. *Annu. Rev. Plant Biol.* **53,** 503–521 (2002).
23. Kuhlbrandt, W., Wang, D. N. & Fujiyoshi, Y. Atomic model of plant light-harvesting complex by electron crystallography. *Nature* **367,** 614–621 (1994).
24. Jansson, S. A. Guide to the Lhc genes and their relatives in *Arabidopsis. Trends Plant Sci.* **4,** 236–240 (1999).
25. Morosinotto, T., Castelletti, S., Breton, J., Bassi, R. & Croce, R. Mutation analysis of Lhca1 antenna complex. Low energy absorption forms originate from pigment–pigment interactions. *J. Biol. Chem.* **277,** 36253–36261 (2002).
26. Moseley, J. L. *et al.* Adaptation to Fe-deficiency requires remodeling of the photosynthetic apparatus. *EMBO J.* **21,** 6709–6720 (2002).
27. Schmid, V. H. *et al.* Pigment binding of photosystem I light-harvesting proteins. *J. Biol. Chem.* **277,** 37307–37314 (2002).
28. Croce, R., Zucchelli, G., Garlaschi, F. M. & Jennings, R. C. A thermal broadening study of the antenna chlorophylls in PSI-200, LHCI, and PSI core. *Biochemistry* **37,** 17355–17360 (1998).
29. Rivadossi, A., Zucchelli, G., Garlaschi, F. M. & Jennings, R. C. The importance of PSI chlorophyll red forms in light-harvesting by leaves. *Photosynth. Res.* **60,** 209–215 (1999).
30. Jennings, R. C., Zucchelli, G., Croce, R. & Garlaschi, F. M. The photochemical trapping rate from red spectral states in PSI-LHCI is determined by thermal activation of energy transfer to bulk chlorophylls. *Biochim. Biophys. Acta* **1557,** 91–98 (2003).
31. Bengis, C. & Nelson, N. Subunit structure of chloroplast photosystem I reaction center. *J. Biol. Chem.* **252,** 4564–4569 (1977).
32. Xue, Y., Okvist, M., Hansson, O. & Young, S. Crystal structure of spinach plastocyanin at 1.7 Å resolution. *Protein Sci.* **7,** 2099–2105 (1998).
33. Sommer, F., Drepper, F. & Hippler, M. The luminal helix l of PsaB is essential for recognition of plastocyanin or cytochrome c6 and fast electron transfer to photosystem I in *Chlamydomonas reinhardtii*. *J. Biol. Chem.* **277,** 6573–6581 (2002).
34. Chitnis, P. R., Purvis, D. & Nelson, N. Molecular cloning and targeted mutagenesis of the gene *psaF* encoding subunit III of photosystem I from the cyanobacterium *Synechocystis* sp PCC 6803. *J. Biol. Chem.* **266,** 20146–20151 (1991).
35. Hippler, M., Drepper, F., Haehnel, W. & Rochaix, J. D. The N-terminal domain of PsaF: precise recognition site for binding and fast electron transfer from cytochrome c6 and plastocyanin to photosystem I of *Chlamydomonas reinhardtii*. *Proc. Natl Acad. Sci. USA* **95,** 7339–7344 (1998).
36. Bibby, T. S., Nield, J. & Barber, J. Iron deficiency induces the formation of an antenna ring around trimeric photosystem I in cyanobacteria. *Nature* **412,** 743–745 (2001).
37. Boekema, E. J. *et al.* A giant chlorophyll–protein complex induced by iron deficiency in cyanobacteria. *Nature* **412,** 745–748 (2001).
38. Nield, J., Morris, E. P., Bibby, T. S. & Barber, J. Structural analysis of the photosystem I supercomplex of cyanobacteria induced by iron deficiency. *Biochemistry* **42,** 3180–3188 (2003).
39. Melkozernov, A. N., Lin, S., Bibby, T. S., Barber, J. & Blankenship, R. E. Time-resolved absorption and emission show that the CP43′ antenna ring of iron-stressed *Synechocystis* sp. PCC6803 is efficiently coupled to the photosystem I reaction center core. *Biochemistry* **42,** 3893–3903 (2003).
40. Nelson, N. & Ben-Shem, A. Photosystem I reaction center: Past and future. *Photosynth. Res.* **73,** 193–206 (2002).

Supplementary Information accompanies the paper on **www.nature.com/nature**.

Acknowledgements We acknowledge the ESRF for synchrotron beam time, and staff scientists of the ID14 stations cluster for their assistance. We thank W. Kuhlbrandt for LHCII coordinates. A.B. is a recipient of a Charles Clore Foundation Ph.D. student scholarship. This work was supported by a grant from The Israel Science Foundation to N.N. and F.F.

Competing interests statement The authors declare that they have no competing financial interests.

Correspondence and requests for materials should be addressed to N.N. (nelson@post.tau.ac.il). Atomic coordinates are deposited in the Protein Data Bank under accession number 1qzv.